Effect of incompressibility on lateral instabilities of polymer brushes in a poor solvent

Christopher Roderick, Hong Guo, and Martin J. Zuckermann
Centre for the Physics of Materials and Department of Physics, McGill University, Montreal, PQ, Canada H3A 2T8
(Received 20 April 2000; published 21 December 2000)

We report a theoretical investigation of the lateral instability of grafted polymer layers in a poor solvent. Within self-consistent mean-field theory, we carry out a linear stability analysis at the random phase approximation level, for which an explicit incompressibility condition is enforced. Our analysis predicts a stability diagram in which regions of stable and unstable polymer brush profiles are located. Compared with analysis where incompressibility is not taken into account, our results suggest that lateral stability is enhanced.

DOI: 10.1103/PhysRevE.63.012501 PACS number(s): 72.10.Bg

Understanding the behavior of dense polymer brushes is a problem of scientific and technological importance which has attracted significant research effort [1]. Of the many aspects of such systems, determining their conformational response to the solvent condition is crucial to the prediction of their physical properties. In a good solvent and with a high grafting density, the chains of a polymer brush overlap repulsively, and stretch away from the substrate [2]. However, when a polymer brush is immersed in sufficiently poor solvent, it becomes energetically unfavorable for the solvent molecules to mix with the polymers [3–6], and a microphase separation occurs where polymers and solvent molecules are spatially separated. A theoretical analysis of polymer brushes under poor solvent conditions was the subject of several previous works [3,4,7,8]. Of particular interest to this paper is the self-consistent field (SCF) analysis due to Yeung, Balazs, and Jasnow [8] (YBJ), who combined the random phase approximation [7] with a numerical SCF, thereby predicting the occurrence of a linear instability of stretched brush configurations as the solvent quality was reduced. It was found that there existed two regimes along the stability line separating the extended and collapsed polymer brushes: a weakly interacting Gaussian regime, where the grafted layer was ''dimpled'' through the depth of the layer; and a regime where the dimpling was confined to the outer tips of the layer.

In this report we present a study of the lateral instability of a polymer brush in a poor solvent where incompressibility is explicitly included. This instability is controlled by the balance between solvation energy and configurational entropy. Theoretical predictions of instability hence depend upon excluded volume effects for which the incompressibility of the system could play an important role. However, this condition was neglected in previous analyses [3,4,8]. Our main result shows that the incompressibility condition has a quantitative influence upon the predicted stability line in the strongly interacting regime.

We consider an effective Hamiltonian for polymer brushes [9],

$$\mathcal{H}[\hat{\rho}_p,\hat{\rho}_s]=\frac{3}{2b^2}\sum_{n=1}^{N_p}\int_0^M d\mu\left[\frac{d}{d\mu}\mathbf{R}_n(\mu)\right]^2 + \alpha\int_V d\mathbf{r}\hat{\rho}_p(\mathbf{r})\hat{\rho}_s(\mathbf{r}), \tag{1}$$

where the temperature has been absorbed into the Hamiltonian and b is the statistical bond length. The parameter $\alpha>0$ controls the polymer-solvent interaction, and thus a larger value of α indicates a poorer solvent quality. N_p is the total number of polymers in the brush, and V refers to the semi-infinite volume $z>0$ ($z=0$ being the grafting plane). The first term of Eq. (1) describes the entropic stretching energy of the chains, where $\mathbf{R}_n(\mu)$ is the position vector of the μth monomer on the nth chain. The grafting of the chains to an impenetrable interface is manifest as the following two constraints on the z components of the monomer positions: $[\mathbf{R}_n(0)]_z=0$ and $[\mathbf{R}_n(\mu)]_z>0$ for $0<\mu\leqslant M$. The second term of Eq. (1) gives the interaction between polymer and solvent in terms of monomer and solvent densities $\hat{\rho}_p$ and $\hat{\rho}_s$, defined as $\hat{\rho}_p(\mathbf{r})\equiv\Sigma_{n=1}^{N_p}\int_0^M d\mu\,\delta[\mathbf{r}-\mathbf{R}_n(\mu)]$ and $\hat{\rho}_s(\mathbf{r})\equiv\Sigma_{i=1}^{N_s}\delta[\mathbf{r}-\mathbf{r}_i]$, respectively, where $\mathbf{r}_i$ is the position of the ith solvent particle, and N_s is the total number of solvent molecules. Finally, our model includes an incompressibility condition. In the mean-field approximation, the incompressibility of a mixture of two materials is expressed by a local conservation law [10],

$$\frac{\rho_p(\mathbf{r})}{\rho_{0p}}+\frac{\rho_s(\mathbf{r})}{\rho_{0s}}=1 \tag{2}$$

where ρ_{0p} and ρ_{0s} are the bulk number densities of pure monomers and solvent, respectively. Model (1) is off lattice, and as a consequence b, the statistical bond length, and $\rho_{0p}^{-1/3}$, relating to the packing diameter of an effective monomer, are independent length scales. Solvent molecules [11] are explicitly included through the configurational density $\hat{\rho}_s(\mathbf{r})$, and the incompressibility condition [Eq. (2)] is included as a constraint throughout our analysis. As the bulk densities are the reciprocal of the solvent molecule and monomer volumes, they effectively control excluded volume interactions, as shown in the virial expansion derived below [Eqs. (6) and (7)].

Our analysis proceeds in two steps. First, we calculate the laterally homogeneous mean-field (MF) solution of the brush profile by a numerical self-consistent calculation following the standard technique [10]. Next we apply the random phase approximation [7,8] (RPA) to expand the free energy functional self-consistently around the MF state, obtaining a stability criteria for the brush against Gaussian fluctuations. The stability analysis gives us the stability boundary which sepa-

rates the stable and unstable brush profiles. The SCF analysis is based on the effective Hamiltonian [Eq. (1)] which defines the partition function by including Eq. (2) as well as making the mean field densities $\rho_p(\mathbf{r})$ and $\rho_s(\mathbf{r})$ equal to $\hat{\rho}_p$ and $\hat{\rho}_s$. These constraints are imposed by the use of undetermined Lagrange multipliers [10] in the standard manner. Application of the method of Hong and Noolandi [10], enables us, after considerable analysis [12], enables us, after considerable analysis, to reduce the partition function to the form

$$\mathcal{Z}=\int \mathcal{D}\{X\}\exp(-H[\{X\}]), \tag{3}$$

where $\mathcal{D}(\cdots)$ denotes functional integration. $\{X\} \equiv[\omega_p,\omega_s,\eta,\rho_p,\rho_s]$ is the collective symbol for mean-field potentials $\omega_p(\mathbf{r})$ of polymers and $\omega_s(\mathbf{r})$ of solvent particles, and the Lagrange multiplier $\eta(\mathbf{r})$ for the incompressibility condition [12] [Eq. (2)]. The effective Hamiltonian H of Eq. (3) has the expression

$$-H[\{X\}]=\ln Q_p[\omega_p]+N_s\ln Q_s[\omega_s]+\int_V d\mathbf{r}[\omega_p(\mathbf{r})\rho_p(\mathbf{r}) + \omega_s(\mathbf{r})\rho_s(\mathbf{r})-\alpha\rho_p(\mathbf{r})\rho_s(\mathbf{r})] + \int_V d\mathbf{r}[1-\phi_p(\mathbf{r})-\phi_s(\mathbf{r})]\,\eta(\mathbf{r}), \tag{4}$$

where Q_p is the polymer Green's function [9] which satisfies a diffusion equation with potential $\omega_p(\mathbf{r})$, $Q_s[\omega_s] \equiv\int_V d\mathbf{r}\exp(-\omega_s(\mathbf{r}))/V$, and, $\phi_{p,s}(\mathbf{r})\equiv\rho_{p,s}(\mathbf{r})/\rho_{0p,0s}$ are the fractional number densities.

Minimization of $H[\{X\}]$ with respect to its variables gives a set of mean-field equations which were solved self-consistently together with the diffusion equation on a numerical grid [12]. Throughout the numerical analysis we fixed the number of monomers per chain at $M=64$, the statistical bond length at $b=\sqrt{3}$, and the grafting density at $\sigma_p=1/5$ (the number of polymer chains per unit area). Figure. 1(a) gives the SCF monomer density profiles in a direction perpendicular to the grafting plane (the z direction) for several values of α. It is clear that the density profile $\rho_p(z)$ is gradually pushed toward the grafting plane as the solvent quality is reduced (α is increased). These results are consistent with those obtained previously [13].

The stability of the density profile in poor solvent was analyzed by investigating the effects of fluctuations within the RPA following a similar procedure to that of Ref. [8]. In our case, we expand the effective Hamiltonian of Eq. (4) around the mean field to second order, and obtain [14] the two-point correlation function for density fluctuations,

$$C^{-1}_{RPA}(\mathbf{r}_1,\mathbf{r}_2)=\frac{1}{4}[\rho^2_{0p}C^{-1}_{pp}(\mathbf{r}_1,\mathbf{r}_2)+\rho^2_{0s}C^{-1}_{ss}(\mathbf{r}_1,\mathbf{r}_2)] - \frac{\alpha\rho_{0p}\rho_{0s}}{2}\delta(\mathbf{r}_1-\mathbf{r}_2), \tag{5}$$

where $C_{pp}(\mathbf{r}_1,\mathbf{r}_2)=\partial^2\ln Q_p[\omega_p]/\partial\omega_p(\mathbf{r}_1)\partial\omega_p(\mathbf{r}_2)$. A similar expression for C_{ss} is found by replacing polymer quantities by solvent quantities. The linear stability of the polymer brush is determined by calculating the eigenvalues of the correlation matrix C^{-1}_{RPA} as a function of the lateral fluctuation wavelength: we vary the interaction parameter α until an eigenvalue becomes zero, signaling the onset of a linear instability of the mean-field brush profile [8]. This analysis is performed for several system parameters ρ_{0s} and ρ_{0p}.

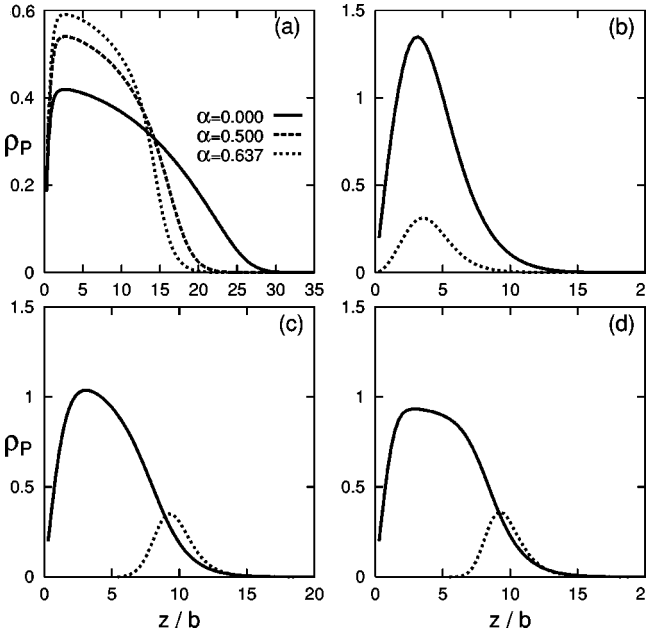

FIG. 1. Density profiles of polymer brush along the direction perpendicular to the grafting surface. (a) Comparison of profiles for different solvent quality for parameters $\rho_{0p}=\rho_{0s}=1$, $\sigma_p=0.2$, and $M=64$. Solid line: a good solvent where the brush is strongly stretched; dashed line: a θ solvent; dotted line: a poor solvent. (b) $\rho_{0p}=6$ and $\rho_{0s}=0.05$. (c) $\rho_{0p}=6$ and $\rho_{0s}=40$. (d) $\rho_{0p}=1$ and $\rho_{0s}=0.05$. For 1(b)–1(d) the other parameters are the same as in (a). The dotted curves of 1(b)–1(d) give the least-stable eigenvectors obtained from the correlation matrix [Eq. (5)]. ρ_p shows units of number of effective monomers per unit volume, and the scaled distance from the grafting surface z/b is dimensionless.

Figures 1(b)–1(d) show the density profiles at the point of instability together with the least stable eigenvector (that with zero eigenvalue) of the correlation matrix. For large ρ_{0p}, the least stable eigenvectors for the fluctuating modes are located deep inside the brush [Fig. 1(b)] for lower values of ρ_{0s}, and move toward the tip of the brush as ρ_{0s} increases [Fig. 1(c)]. This behavior is consistent with that found by YBJ, corresponding to the Gaussian and stretched conformations, respectively [8]. On the other hand, for small ρ_{0p} [Fig. 1(d), where $\rho_{0p}=1$], the least stable eigenmode must locate in the tip region because fluctuations in the center of the layer would bring the monomers into closer contact where excluded volume interactions would stabilize the layer. The fact that the least stable mode is located inside the layer [Fig. 1(b)] indicates the onset of the ''dimpled phase'' where large density fluctuations would span the entire brush. On the other hand, when the least stable mode is near the tip region, the dimpling is localized at the outer part of the brush [8].

Figure 2 shows slices through the stability surface sepa-

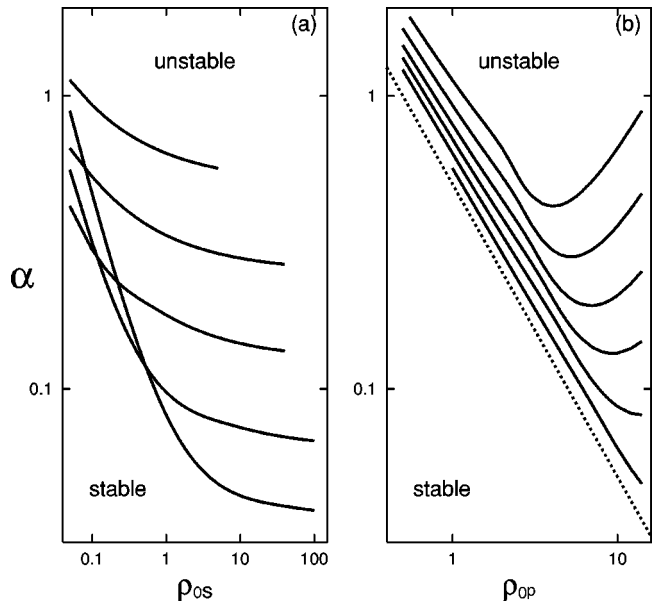

FIG. 2. Stability lines: For each case, the stable region lies below the line, while the linearly unstable region lies above the line for the extended brush profiles. Panel (a): α vs ρ_{0s} for $\rho_{0p}=1,2,4,8$, and 14 (top to bottom). Panel (b): α vs ρ_{0p} for $\rho_{0s}=0.05,0.1,0.2,0.4,1,5$, and 100 (top to bottom), with the dotted line representing a Θ solvent [$\alpha=1/(2\rho_{0p})$]. ρ_{0p} shows units of number of effective monomers per unit volume, ρ_{0s} units of number of solvent particles per unit volume, and α units of volume.

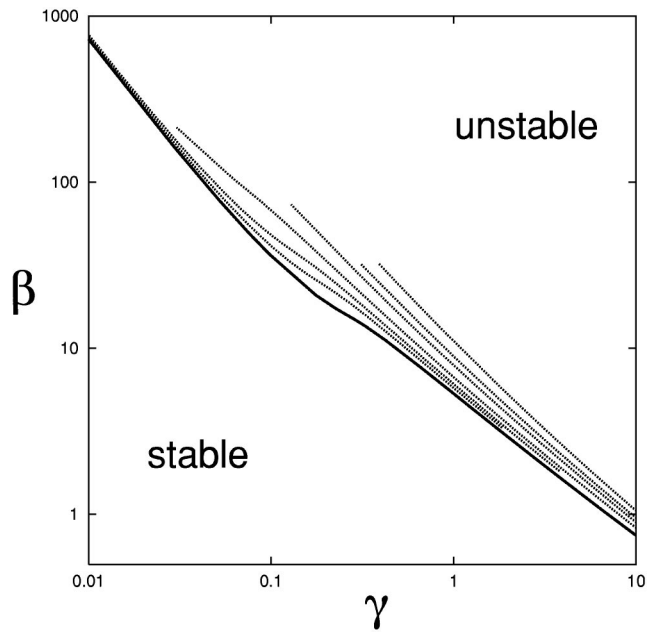

FIG. 3. Comparison of the stability lines between models (1) and (6) using the variables γ and β. The solid line corresponds to the model (6) which does not explicitly include incompressibility. The dotted lines correspond to the model [Eqs. (1) and (2)] obtained by fixing $\rho_{0p}=0.75,1.1,1.5,2.75,5.0$, and 9.0 from top to bottom. Both γ and β are dimensionless, as noted in the body of the text where they are defined.

rating the extended brush regime from the collapsed brush regime. Fig. 2(a) indicates that for fixed ρ_{0p}, a smaller value of the interaction parameter α is required to drive the instability as ρ_{0s} is increased. This is understandable since a larger value of ρ_{0s} means smaller solvent molecules, which can more easily penetrate into the grafted layer. As a direct consequence of the model Hamiltonian [Eq. (1)], where the overlap of solvent and monomer densities directly determine the interaction, a larger overlap requires a smaller value of α to drive the instability. This trend is diminished when ρ_{0p} is decreased, as shown by the successive constant ρ_{0p} lines in Fig. 2(a). The reason is the same: for larger volume per monomer (smaller ρ_{0p}) there is less free volume in the layer into which the solvent molecules can penetrate, diminishing the overlap and enhancing the stability. This physical picture is consistent with Fig. 2(b), where the stability lines are plotted for constant ρ_{0s}, in the regime of small ρ_{0p}. The regime of large ρ_{0p} shall be discussed shortly.

It is useful to compare our analysis with that of Ref. [8], which was based on a virial expansion of the Hamiltonian. In order to do so, we first integrate out quantities related to the solvent molecules, ω_s, ρ_s, and η from the partition function [Eq. (3)] using the mean-field equations. The result, truncated at third order, is [12]

$$\mathcal{H}[\omega_p,\rho_p]=-\ln Q[\omega_p]-\int_V d\mathbf{r}\omega_p(\mathbf{r})\rho_p(\mathbf{r}) + \frac{w_2}{2}\int_V d\mathbf{r}\rho_p^2(\mathbf{r})+\frac{w_3}{3}\int_V d\mathbf{r}\rho_p^3(\mathbf{r}), \qquad (6)$$

where the virial coefficients are found to be

$$w_2=(\rho_{0s}/\rho_{0p}^2)(1-2\alpha\rho_{0p}), \qquad (7)$$

and $w_3=\rho_{0s}/2\rho_{0p}^3$. The first two terms of Eq. (6) give the polymer entropic contribution, while the other terms give the effective interaction between polymers. Clearly, from Eq. (7) the parameter w_2 can be positive, describing a good solvent, or negative, describing a poor solvent, depending on the interaction strength α. On the other hand, the parameter w_3, and all the omitted higher order coefficients, are positive [15]. Our model [Eqs. (1) and (2)] is equivalent to the full virial expansion when no terms are omitted. Equation (7) indicates that the θ solvent ($w_2=0$) is given by $\alpha=1/(2\rho_{0p})$, corresponding to the dotted line shown in Fig. 2(b). In addition, fixing the interaction strength α, w_2 is negative when $\rho_{0p}>1/(2\alpha)$, indicating a poor solvent. Minimization of w_2 with respect to ρ_{0p} in Eq. (7) gives the most negative value of w_2 when $\rho_{0p}=1/\alpha$. Hence, when taking into account the entropic contribution to the free energy, we expect the linear stability line to change behavior near $\rho_{0p}=1/\alpha$. Figure 2(b) shows that this is indeed the case as the unstable region shrinks when ρ_{0p} becomes large, as indicated by the upward bend of the stability line.

The Hamiltonian of Eq. (6) was used in Ref. [8] to analyze the stability of polymer brushes in a poor solvent. It was shown [8] that the linear stability is characterized by two dimensionless parameters γ and β, defined as $\gamma=3M(\sigma/b)^2(w_3/w_2)^2$ and $\beta=(1/3)(b/\sigma)^2(w_2^4/w_3^3)$. Here γ gives a measure of the stretching of the brush away from

the grafting surface relative to the lateral extent of a Gaussian chain, and β is the strength of the interaction relative to the stretching energy of a chain. We performed the stability analysis using Hamiltonian (6), confirming the result of Ref. [8], and compared the stability lines of both models [Eqs. (1), (2) and Eq. (6)] as shown in Fig. 3. Several comments are in order.

First, the result without explicit inclusion of the incompressibility condition, i.e., using Hamiltonian (6), is given by the limiting stability line as indicated by the solid curve. This is understandable, since solvent incompressibility imposes a constraint on the local solvent density, thereby reducing the interaction between solvent and polymer. For this reason, our model [Eqs. (1) and (2)] always gives a larger stable region as shown in Fig. 3. Second, the stability lines in Fig. 3 of our model [Eqs. (1) and (2)] were calculated by fixing ρ_{0p}, and varying ρ_{0s} and α. Consistent with Fig. 2(a), smaller values of ρ_{0p} give larger regions with a stable extended brush profile. This is indicated by the dotted lines above the solid line in Fig. 3. This is also consistent with Eq. (7) where a smaller value of ρ_{0p} can make the parameter w_2 less negative giving a slightly better solvent condition. Third, in the weak interaction regime where γ is small, our results are in good agreement with Ref. [8], and confirm the $\beta \propto \gamma^{-3/2}$ scaling of the stability line (see Fig. 3). In this regime, the least stable fluctuating mode is located inside the brush as shown in Fig. 1(b), and it leads to the ''dimple'' profile discussed in Ref. [8]. Finally, in the strongly interaction regime where γ is large, the model of Eq. (6) gives a scaling of $\beta \propto \gamma^{-3/4}$, while our model asymptotically approaches this exponent from below. In this regime, the least stable modes are located near the tip of the brush as shown in Figs. 1(c) and 1(d). This indicates that the dimpling occurs near the outer tip of the polymer layer [8].

In summary, we have examined the linear stability of a polymer brush in a poor solvent under the constraint of incompressibility. Our results, based on the model of Eq. (2,1), give qualitatively the same physical picture [8] obtained from a simpler model of Eq. (6). Specifically, there exist two regimes of the linear stability: the weak and strong interaction limits. In the former, where incompressibility is essentially not important due to weak interaction, both models are quantitatively equivalent. In the latter, where incompressibility plays a role, there is a quantitative change to the stability line obtained from the simpler model of Eq. (6): our model predicts a larger region for stable polymer brush profiles in the ''phase'' diagram of Fig. 3.

The authors gratefully acknowledge Dr. G. Soga, Dr. J. Polson, Professor M. Laradji, Professor C. Yeung, Professor D. Jasnow, Professor A. Balacz, and Professor M. D. Whitmore for many useful discussions on SCF and RPA theories. We acknowledge financial support from NSERC of Canada and FCAR of Quebec (H. G. and M. Z.).

[1] S.T. Milner, Science **251**, 905 (1991). For a recent review, see Y. Uyama, K. Kato, and Y. Ikada, Adv. Polym. Sci. **137**, 1 (1998); R.R. Netz and D. Andelman, e-print cond-mat/0002266.

[2] P.G. de Gennes, Macromolecules **13**, 1069 (1980).

[3] A. Halperin, J. Phys. (France) **49**, 547 (1988); P.Y. Lai and K. Binder, J. Chem. Phys. **97**, 586 (1992); G.S. Grest and M. Murat, Macromolecules **26**, 3108 (1993); E.B. Zhulina, T.M. Birshtein, and V.A. Priamitsyn, *ibid.* **27**, 418 (1994); H. Tang and I. Szleifer, Europhys. Lett. **28**, 19 (1994).

[4] K.G. Soga, H. Guo, and M. Zuckermann, Europhys. Lett. **29**, 531 (1995).

[5] P. Auroy and L. Auvray, Macromolecules **25**, 4134 (1992).

[6] D.F. Siqueria, K. Köler, and M. Stamm, Langmuir **11**, 3092 (1995).

[7] R.S. Ross and P. Pincus, Europhys. Lett. **19**, 79 (1992).

[8] C. Yeung, A.C. Balazs, and D. Jasnow, Macromolecules **26**, 1914 (1993).

[9] K.F. Freed, Adv. Chem. Phys. **22**, 1 (1972).

[10] K.M. Hong and J. Noolandi, Macromolecules **14**, 727 (1981); **14**, 1229 (1981).

[11] By integrating Eq. (2) over the system volume V, one finds that the number of solvent particles is $N_s = \rho_{0s}(V - MN_p/\rho_{0p})$. For all our simulations V and the total number of monomers MN_p are held fixed, and N_s is allowed to vary. This is acceptable, since it is the number of solvent particles that penetrate into the grafted layer [the second term of Eq. (1)], and not the total number in the system, that affects the stability of the layer. This is controlled by the size $1/\rho_{0s}$ of individual solvent particles.

[12] C. Roderick, Ph.D. thesis, McGill University, 2001 (unpublished).

[13] M.D. Whitmore and J. Noolandi, Macromolecules **23**, 3321 (1990).

[14] A detailed account of a similar derivation was given by A. C. Shi, J. Noolandi, and R. C. Desai, Macromolecules **29**, 6487 (1996).

[15] The higher order virial coefficients are found to be $w_n = \rho_{0s}/[(n-1)\rho_{0p}^n]$ for $n \geqslant 3$.